Nanoscale

Three-Dimensional Directed Assembly of Organic Charge-Transfer Heterostructures

Journal:	*Nanoscale*
Manuscript ID	NR-ART-09-2018-007878.R1
Article Type:	Paper
Date Submitted by the Author:	12-Nov-2018
Complete List of Authors:	Zhang, Lin; University at Buffalo - The State University of New York Hu, Yong ; University at Buffalo - The State University of New York Chang, Shuquan; Nanjing University of Aeronautics and Astronautics, College of Materials Science and Technology; Nanjing University of Aeronautics and Astronautics, Jiangsu Engineering Laboratory of Nuclear Energy Equipment Materials Guan, Yingshi; University at Buffalo - The State University of New York Ren, Shenqiang; University at Buffalo - The State University of New York,

Journal Name

ARTICLE

Three-Dimensional Directed Assembly of Organic Charge-Transfer Heterostructure

Received 00th January 20xx,
Accepted 00th January 20xx

DOI: 10.1039/x0xx00000x

www.rsc.org/

Lin Zhang,[1,#] Yong Hu,[1,#] Shuquan Chang,[2] Ying-Shi Guan,[1] and Shenqiang Ren[1,*]

Multicomponent crystalline heterostructures are a powerful approach to integrate different functional materials into the ordered structures. Here we describe three-dimensional spherical assembly of binary organic solids that consist of electron donor and acceptor molecules. A mechanistic study of heterostructure formation reveals that the dewetting and drying-mediated assembly processes are responsible for the spherical crystallite formation. The assembled spherical heterostructures are highly tunable, crystalline and chemically stable, exhibiting phase separation controlled optoelectronic behavior. This simple, generalizable three-dimensional assembly can be modified for the formation of ordered functional organic multicomponent heterostructures for emerging applications.

1 Introduction

Various attempts have been made to prepare organic hierarchical nanostructured solids with tunable optical, magnetic, electric and optoelectronic properties.[1-4] Three-dimensional (3D) assembly of organic charge-transfer (CT) complexes is an important strategy to integrate electron donor and acceptor building blocks to yield multifunctional metamaterials arising from the collective behaviors.[5-7] Besides using Bridgman and Czochralski crystal growth, high-quality organic crystalline heterostructures can also be prepared from solution or physical vapor transport through the intermolecular interaction, e.g. van der Waals forces.[7-11] Recent developments in self-assembled organic heterostructures have considerably extended the range of molecular interactions, therefore allowing structures with the tailored geometries and dimensions.[12-15] Such material assemblies showcase promising applications,[16-19] but can also provide a fundamental understanding of molecular CT interaction controlled unusual physicochemical properties,[20] which can often exhibit distinct electron transfer, dipolar and spin ordering, as well as external stimuli controlled behavior.[21-23] Although fullerene based CT assemblies possess extraordinary physical properties,[24-29] an extension to 3D heterostructures is not trivial and has consequently remained unexploited.[30-32] Such 3D heterostructures would, however, allow charge transfer complexation, which has an essential effect on their electronic, optical and magnetic properties. Here we present a new 3D assembly strategy for the growth of organic polythiophene-C_{60} CT heterostructures. The vapor pressure and the concentration of anti-solvent, as well as the annealing temperature allow CT heterostructure formation with the size and morphology control, and we show that the heterostructures are responsive to external stimuli, such as phase separation controlled optoelectronic properties.

2 Experimental Section

2.1 Materials and three-dimensional assembly

Polythiophene (poly(3-hexylthiophene): P3HT) (7mg/ml) [regioregularity (RR) of 96.3% (HRR) and 91%(LRR)] was dissolved in 1,2-dichlorobenzene (1,2-DCB) under 65 °C for 3 hours. The C_{60} was added into the solution at a weight ratio of 1:3 (P_3HT/C_{60}) and stirred under room temperature for 12 hours. The solution was stored in the nitrogen glovebox before using. The SiO_2/Si substrate was cleaned by successively sonicated in soap solution, distilled water, acetone and isopropanol and dried under N_2 atmosphere, and followed by the ultraviolet/ozone treatment for 15 min. After cleaning, 10 µL P_3HT-C_{60} solution was drop-coasted onto the substrate in a sealed vial, a selective volume of anti-solvent was dropped in the vial. The sealed vial was then heated on the hotplate at a controlled temperatures for 40 min. HRR polythiophene was purchased from Ossila Ltd. (M104, RR=96.3%, Mw=77,500, Mn=38,700). LRR polythiophene was purchased from BASF in cooperation with Rieke Metals (Sepiolid P200, RR=91%, Mw average = 50 to 70 K). The C_{60} (purity, 99.5%) was purchased from Sigma-Aldrich.

2.2 Device using self-assembled structures

[1] Department of Mechanical and Aerospace Engineering
University at Buffalo, The State University of New York
Buffalo, NY 14260, USA
[2] College of Material Science and Technology, Nanjing University of Aeronautics and Astronautics, Nanjing 210016, China
[#] L. Zhang, and Y. Hu contribute equally to this work.
E-mail: shenren@buffalo.edu
†Electronic Supplementary Information (ESI) available: Optical microscopy images, SEM images and photoresponse behavior data are included in the supporting information. See DOI: 10.1039/x0xx00000x

Poly(3,4-ethylenedioxythiophene):polystyrene sulfonate (PEDOT:PSS) was spun-cast onto a 12 × 12 mm^2 glass substrate with prepatterned (1 cm × 1 cm) ITO electrodes. The coated-devices was then heated under 150 °C for 30 min. A certain amount of P_3HT-C_{60} was dissolved in the dimethylformamide (DMF) solvent at a weight ratio of 1:1. The 50 µL suspension was drop-casted on the devices. When the devices were naturally dried at room temperature under N_2 atmosphere, 10 nm bathocuproine (BCP) hole blocking layer and 100 nm Al electrode were evaporated. Current-voltage (J-V) characteristics of the devices were measured with a CHI 422 Series Electrochemical Workstation with and without the illumination. The UV-Vis spectrum was recorded using an Agilent Model HP8453 UV-vis spectrophotometer. Room temperature X-ray diffraction was obtained using monochromated Cu-Ka radation on a Bruker diffraction system. The scanning electron microscopy (SEM) and energy-dispersive X-ray spectroscopy (EDS) element mapping were done with a Hitachi S3400N SEM equipped with EDS.

3 Results and Discussion

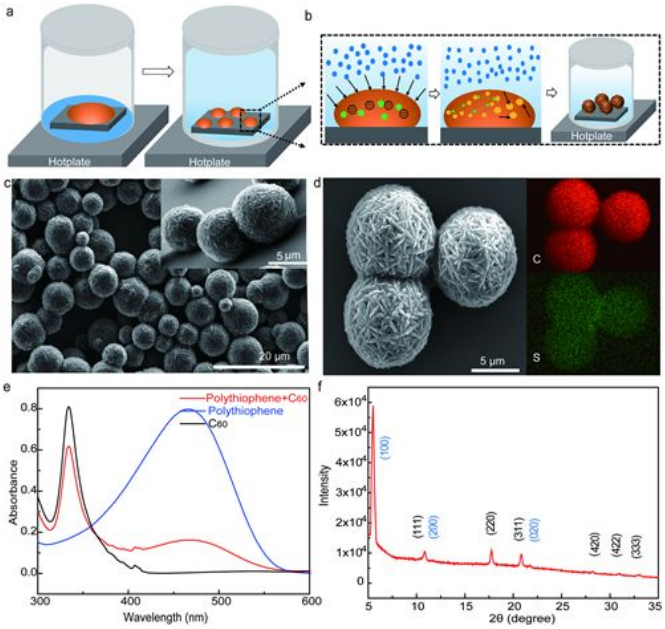

Figure 1. (a) Schematic solvent annealing process for the formation of organic CT heterostructures. (b) Crystallization and solidification processes under saturated solvent vapor. (c) Top-view and side-view (shown in the inset) scanning electron microscope (SEM) images of polythiophene-C_{60} formed at 313K under 30 µL ACN atmosphere. (d) SEM image and the carbon and sulfur EDS elemental mapping from polythiophene-C_{60}, (e) Normalized photoabsorption spectra of C_{60}, polythiophene and polythiophene-C_{60} complex. (f) The XRD spectrum of polythiophene-C_{60} heterostructures.

The solvent vapor diffusion combined with the crystallization is developed to grow multicomponent 3D CT assemblies, consisting of electron donor polythiophene and acceptor C_{60}, in which the polythiophene-C_{60} blended solution is uniformly coated on the substrate and then exposed to a saturated anti-solvent vapor (Fig. 1a). As a result, the dewetting induces the uniform solution film to form the polythiophene-C_{60} droplets (Fig. S1a), the nucleation starts and the miscible fluid flowing makes the nucleus agglomeration under the impact of vapor pressure (Fig. 1b). Simultaneously, the nucleus absorbs the surrounding precursor for the further crystallization of polythiophene-C_{60} assembly. Finally, the coalescence of the seed crystals results in the final spherical agglomeration to reduce the total surface energy (Fig. S1b and S1c). The well-defined spherical polythiophene-C_{60} heterostructures are highly reproducible (Fig. 1c and Fig. S1d). Fig. 1d and Fig.S2 show the elemental mapping image using energy-dispersive X-ray spectroscopy (EDS), where the uniform distribution of sulfur content in the spherical structure suggests the co-crystalline nature from the polythiophene and C_{60} components. In addition, the presence of polythiophene in the spherical heterostructure is evident by its distinct photoabsorption peaks due to the aromatic-aromatic interactions and its high packing density in the co-crystalline structure (Fig. 1e). Furthermore, the X-ray diffraction spectrum (XRD, Fig. 1f) confirms the crystalline structure of polythiophene and C_{60} components. The three distinct diffraction peaks at 5.3°, 10.7° and 23.4° are corresponding for the crystallographic (100), (200) and (020) reflections of polythiophene, respectively, which are attributed by its monoclinic structure (a=1.717 nm, b=0.77 nm, c=0.836 nm).[33] The face centered cubic (fcc) lattice structure of C_{60} with a lattice constant of 1.415 nm is supported by the (111), (220), (311), (420), (422) and (333) reflections.[34]

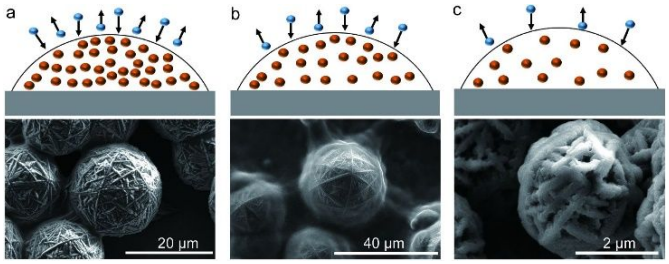

Figure 2. The SEM images of polythiophene-C_{60} heterostructures formed at 313K under anti-solvent vapor atmosphere produced by (a) 30 µL ACN, (b) 30 µL Toluene, (c) 30 µL DMF.

The crystallization induced morphology and dimension control of polythiophene-C_{60} CT heterostructures are largely influenced by the annealing temperature, anti-solvent vapor pressure and concentrations. Particularly, the vapor pressure of anti-solvent determines the number of molecules penetrating into polythiophene-C_{60} droplets to control their crystallization. Three different anti-solvents - acetonitrile (ACN), toluene and dimethylformamide (DMF) - are selected to examine the vapor pressure effect on the crystallization of CT heterostructures, where the ACN has the highest vapor pressure (169.7 torr) followed by toluene (58.08 torr) and DMF (48.07 torr) anti-solvents at 313 K.[35-37] Therefore, the absolute amount of anti-solvent molecules penetrated into the droplet for nucleation can be controlled. As shown in the Fig. 2a, a high population of

subunits in 3D heterostructures is observed for the anti-solvent ACN, while toluene and DMF anti-solvents yield a relatively low density of the subunits within the assembled structure (Fig. 2b-2c). These results suggest that the anti-solvent with high vapor pressure could provide a large amount of molecules for the nucleation and further subunit growth. This has been verified by adjusting the concentrations of anti-solvent. Based on the Ra-oult's law, the solvent vapor pressure is related to the solvent volume at a certain temperature.[38] Therefore, an increase of the anti-solvent ratio results in a larger amount of subunits to form the spherical 3D crystals, as shown in Fig. S3.

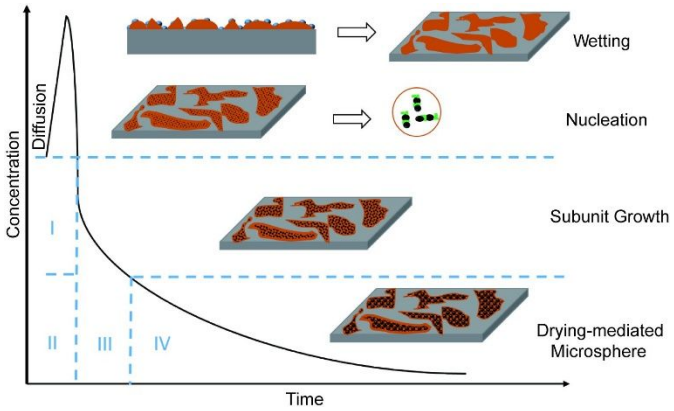

Figure 3. Schematic of the growth model of three-dimensional charge transfer heterostructures

We attribute the growth of micrometer-sized 3D CT heterostructures to the following mechanism (Fig. 3): the dewetting effect of the saturated anti-solvent vapor, the nucleation of polythiophene-C_{60} droplet, further aggregation of nucleus for subunit growth within one droplet and solvent evaporation for the formation of drying-mediated microsphere. In the stage I, as the evaporation of anti-solvent vapor saturates the growth environment, polythiophene-C_{60} droplets are formed due to the dewetting effect, as shown in Fig. 3. During the stage II, as the solvent molecules diffuse into the polythiophene-C_{60} droplet, the C_{60} and polythiophene molecules participate in the formation of nucleus due to the oversaturated interface between the good solvent and anti-solvent.[39,40] In the stage III, within the droplet, the C_{60} molecules aggregate to form the fcc structure while polythiophene chains are stacked in the monoclinic structure through the π-π conjugated interactions. Furthermore, the polythiophene donor and C_{60} acceptor organize themselves for the subunit growth in the form of co-crystalline heterostructures due to intermolecular interactions. Finally, in the stage IV, the agglomeration of co-crystalline heterostructures is occurred, which is driven by the drying-mediated assembly.[41] During the spherical crystal-lization, the nucleation and the subunit growth are two key factors. External stimuli play an important role in controlling the crystalline polythiophene-C_{60} heterostructures in terms of their purity, size and morphology.

The growth of 3D polythiophene-C_{60} heterostructures can be tuned by the vapor pressure of anti-solvent driven by the annealing temperature. As shown in Fig. 4a, the growth rates for C_{60} and polythiophene are nearly identical to create flake-like subunits at the temperature of 313K. As increasing the temperature to 333K, the surface of spherical polythiophene-C_{60} heterostructures is consisted of a large population of closely packed hexagonal prisms (Fig. 4b), and the volume of each prism is up to the maximum when the temperature is increased to 343K (Fig. 4c). This is resulted from a mismatched growth rate of C_{60} than that of polythiophene, as increasing the vapor pressure of anti-solvent. In this context, a surface phase segregation of C_{60} is generated in the stage II, and therefore a distinct change in surface morphology of the spherical heterostructures is occurred, leading to the dominant C_{60} crystallization on the surface (Fig. 4c).

However, as further increasing the temperature to 363K, the volume of hexagonal prims is decreased (Fig. S4a) and the flake-like subunit structures are dominant (Fig. 4d). It should be noted that the temperature is above 343K, the nucleation in the stage II domi-nates where a large number of nucleus is generated because of high vapor pressure of anti-solvent. Therefore, the growth rate difference between polythiophene and C_{60} has less effect on the morphology control at a high annealing temperature. In addition, the average size of spherical heterostructures is increased as increasing the temperature from 313K to 343K, which could be resulted from high vapor pressure induced large amount of subunits (Fig. S4b). However, when the number of the nucleus is saturated at 343K, the average size of the spherical polythiophene-C_{60} heterostructures decreases as further increasing temperature because the polythiophene-C_{60} droplet cannot sustain the further growth of subunits. Based on the above results, we confirm that the morphology and size of the spherical CT heterostructures can be controlled by tuning external temperatures. In addtion, comparing with the XRD spectrum (Fig. S5) and photoabsorption spectra (Fig. S6) of polythiophene-C_{60} heterostructures formed at 313K under 30 μL ACN atmosphere , polythiophene-C_{60} heterostructures formed at 343K under the same atmosphere shows some differences. The XRD spectrum of polythiophene-C_{60} heterostructures formed at 343K indicates that the amorphous polythiophene phase was formed. The absorption peak at 335 nm for polythiophene-C_{60} heterostructures formed at 313K shift to 339 nm for polythiophene-C_{60} heterostructures formed at 343K, suggesting the enhanced charger transfer interaction.

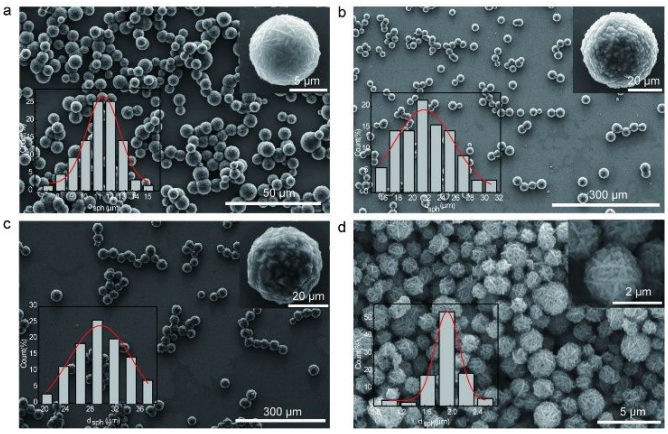

Figure 4. The SEM images of three-dimensional polythiophene-C_{60} heterostructures formed under ACN anti-solvent vapor atmosphere at (a) 313K, (b) 333K, (c) 343K and (d) 363K. The inset is high-magnification SEM image and size distribution of the spherical heterostructures.

To investigate the structure and morphology controlled photoconductive properties of 3D polythiophene-C_{60} CT heterostructures, we select one single spherical heterostructure formed at 313K and 343K for photoresponse measurement as presented in Fig. 5a. Current density-voltage (J-V) curves (Fig. 5b) show that the heterostructures processed at 343K show 10^2 times higher of photoconductivity than that of 313K processed one, which further confirms high mobility surface dominant C_{60} phase annealed at 343K (Fig. 4c). In addition, the heterostructures processed at 343K exhibit a higher light intensity and voltage dependent photoresponse (Fig. 5c-5f, Fig. S7 and S8). As increasing the light intensity (P), the photocurrent (J) can be fitted by the fitting law $J \approx P^{\theta}$ (Fig. S9). The fitting produces a nearly linear relationship for heterostructures formed at 343K suggesting the absence of bimolecular recombination and space limited charges, while the non-unity exponent for the heterostructure annealed at 313K indicates electron-hole generation, recombination and trapping within the heterostructure.[42-44] Consequently, the on-off ratio of heterostructures processed at 343K is as high as 10^3, which is more than one order of mag-nitude larger than that of 313K. The photoresponsibility is calculated according to equation 1:

$$R_i = [J_{(light)}-J_{(dark)}]/p \quad (1)$$

in which J_{light} is the photocurrent density, J_{dark} is the current density under dark and p is the input light power density. It can be seen from Table S1 that the highest R_i is 0.43 mA/w of the heterostructure formed at 343K. In comparison, the heterostructure annealed at 313K exhibits relatively lower photoresponsibility. Similarly, as increasing external voltage from 1.0V to 3.5V, the on/off ratio of heterostructures annealed at 343K is much larger than that of the heterostructures formed at 313K (Fig. 5f). It should be noted that organic CT complexes with the C_{60}-rich phase segregation can lead to a strong interchain interactions for enhanced charge mobility.[45,46] Therefore, the optimum photoresponse of the heterostructures annealed at 343K can be resulted from the phase separation of vertical concentration gradients, leading to high charge carrier mobility and charge transfer interactions.

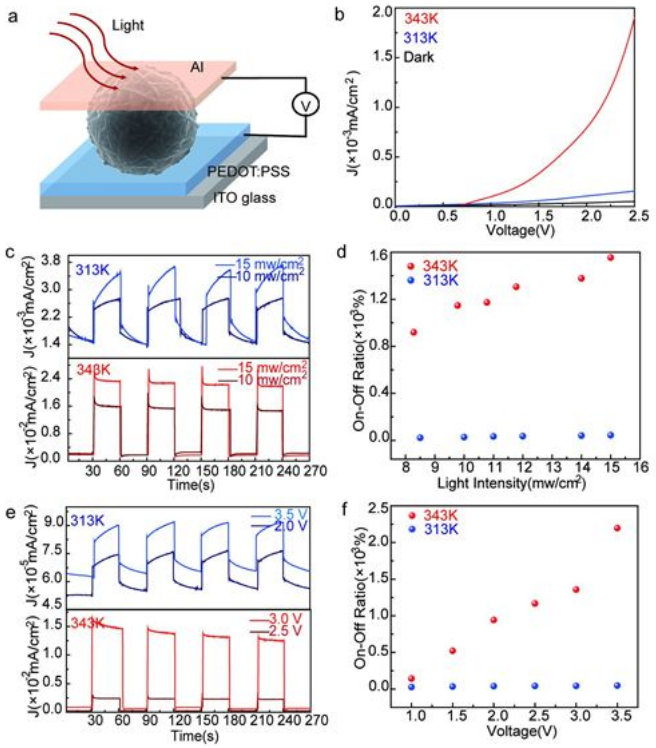

Figure 5. (a-b) The schematic device and J-V curves of polythiophene-C_{60} heterostructures under dark and solar illumination of 12 mw/cm^2. (c-d)The photoresponse and the on-off ratio of heterostructures under solar illumination from 8.5 to 15 mw/cm^2 at 2.5 V. (e-f) The photoresponse and on-off ratio of polythiophene-C_{60} heterostructures under external voltages from 1.0 V to 3.5 V and solar illumination 12 mw/cm^2.

Conclusion

In summary, 3D assembly of organic charge-transfer heterostructures is driven by anti-solvent annealing induced dewetting and crystallization. The structure ordering and crystallization of charge-transfer complexes are controlled through the weak intermolecular interactions, such as π-π stacking, CT and van der Waals forces. By employing different anti-solvents, 3D spherical polythiophene-C_{60} heterostructures with various subunit density are obtained due to the changes of solvent molecules penetrating into the solution. In addition, the size and morphology of 3D CT heterostructures could be controlled by external stimuli, such as the vapor pressure of anti-solvent and solvent annealing temperature. The photoresponse of polythiophene-C_{60} heterostructures are strongly enhanced due to the vertical concentration gradients from phase separation. This 3D assembly approach demonstrates its use with organic charge-transfer complexes, thus paving the way for the successful implementation of multicomponent heterostructures in functional devices.

Acknowledgements

L. Zhang, Y. Hu and Y.-S. Guan contribute equally to this work.

L. Zhang, Y. Hu and Y.-S. Guan contribute equally to this work. Financial support was provided by the U.S. Army Research Office supports S.R. under Award W911NF-18-2-0202.

Notes and references

1 V. Percec, M. Glodde, T. Bera, Y. Miura, I. Shiyanovskaya, K. Singer, V. Balagurusamy, P. Heiney, I. Schnell and A. Rapp, *Nature,* 2002, **419**, 384-387.
2 W. Zhu, R. Zheng, X. Fu, H. Fu, Q. Shi, Y. Zhen, H. Dong and W. Hu, *Angewandte Chemie International Edition,* 2015, **54**, 6785-6789.
3 T. W. Ng, M. F. Lo, M. K. Fung, W. J. Zhang and C. S. Lee, *Advanced Materials,* 2014, **26**, 5569-5574.
4 H. Xu, R. Chen, Q. Sun, W. Lai, Q. Su, W. Huang and X. Liu, *Chemical Society Reviews,* 2014, **43**, 3259-3302.
5 C. Wang, S. Yin, S. Chen, H. Xu, Z. Wang and X. Zhang, *Angewandte Chemie,* 2008, **120**, 9189-9192.
6 R. Chakrabarty, P. S. Mukherjee and P. J. Stang, *Chemical reviews,* 2011, **111**, 6810-6918.
7 H. Jiang and C. Kloc, *MRS bulletin,* 2013, **38**, 28-33.
8 J. Bleay, R. M. Hooper, R. S. Narang and J. N. Sherwood, *Journal of Crystal Growth,* 1978, **43**, 589-596.
9 N. Karl, *Molecular Crystals and Liquid Crystals,* 1989, **171**, 157-177.
10 D. H. Kim, D. Y. Lee, H. S. Lee, W. H. Lee, Y. H. Kim, J. I. Han and K. Cho, *Advanced Materials,* 2007, **19**, 678-682.
11 Y. S. Zhao, H. Fu, A. Peng, Y. Ma, Q. Liao and J. Yao, *Accounts of chemical research,* 2009, **43**, 409-418.
12 H. Zheng, Y. Li, H. Liu, X. Yin and Y. Li, *Chemical Society Reviews,* 2011, **40**, 4506-4524.
13 L. C. Palmer and S. I. Stupp, *Accounts of chemical research,* 2008, **41**, 1674-1684.
14 A. C. Grimsdale and K. Müllen, *Angewandte Chemie International Edition,* 2005, **44**, 5592-5629.
15 T. Hasegawa and J. Takeya, *Science and Technology of Advanced Materials,* 2016, **10**, 024314.
16 A. P. Kulkarni, C. J. Tonzola, A. Babel and S. A. Jenekhe, *Chemistry of materials,* 2004, **16**, 4556-4573.
17 H. Klauk, *Chemical Society Reviews,* 2010, **39**, 2643-2666.
18 H. Hoppe and N. S. Sariciftci, *Journal of Materials Research,* 2004, **19**, 1924-1945.
19 Y. Li, T. Liu, H. Liu, M.-Z. Tian and Y. Li, *Accounts of chemical research,* 2014, **47**, 1186-1198.
20 H. Miyasaka, *Accounts of chemical research*, 2012, **46**, 248-257.
21 T. Yamamoto, *NPG Asia Materials,* 2010, **2**, 54-60.
22 W. Qin, X. Chen, J. Lohrman, M. Gong, G. Yuan, M. Wuttig and S. Ren, *Nano Research,* 2016, **9**, 925-932.
23 A. Laiho, R. H. Ras, S. Valkama, J. Ruokolainen, R. Österbacka and O. Ikkala, *Macromolecules,* 2006, **39**, 7648-7653.
24 K. Itaka, M. Yamashiro, J. Yamaguchi, M. Haemori, S. Yaginuma, Y. Matsumoto, M. Kondo and H. Koinuma, *Advanced Materials,* 2006, **18**, 1713-1716.
25 L. Wei, Y. Wu, L. Wang, H. Fu and J. Yao, *The Journal of Physical Chemistry C,* 2011, **115**, 21629-21634.
26 P. W. Blom, V. D. Mihailetchi, L. J. A. Koster and D. E. Markov, *Advanced Materials,* 2007, **19**, 1551-1566.
27 S. S. Babu, H. Möhwald and T. Nakanishi, *Chemical Society Reviews,* 2010, **39**, 4021-4035.
28 H. Li, B. C. Tee, J. J. Cha, Y. Cui, J. W. Chung, S. Y. Lee and Z. Bao, *Journal of the American Chemical Society,* 2012, **134**, 2760-2765.
29 L. Kang, H. Fu, X. Cao, Q. Shi and J. Yao, *Journal of the American Chemical Society,* 2011, **133**, 1895-1901.
30 L. Kang, Z. Wang, Z. Cao, Y. Ma, H. Fu and J. Yao, *Journal of the American Chemical Society,* 2007, **129**, 7305-7312.
31 L. Huang, Q. Liao, Q. Shi, H. Fu, J. Ma and J. Yao, *Journal of Materials Chemistry,* 2010, **20**, 159-166.
32 B. Xu, H. Li, A. Hall, W. Gao, M. Gong, G. Yuan, J. Grossman and S. Ren, *Science Advances,* 2015, **1**, e1501264.
33 L. Wang, B. Liu, D. Liu, M. Yao, Y. Hou, S. Yu, T. Cui, D. Li, G. Zou and A. Iwasiewicz, *Advanced Materials,* 2006, **18**, 1883-1888.
34 J. Dojcansky and J. Heinrich, *Chem. Zvesti,* 1974, **28**, 157-159.
35 E. B. Munday, J. C. Mullins and D. D. Edie, *Journal of Chemical and Engineering Data,* 1980, **25**, 191-194.
36 E. P. Juárez-Camacho, M. E. Manríquez-Ramírez, C. M. Reza-San Germán and A. Zúñiga-Moreno, *Journal of solution chemistry,* 2012, **41**, 1575-1586.
37 E. Guggenheim, *Transactions of the Faraday Society,* 1937, **33**, 151-156.
38 D. Kim, J. T. Han, Y. Park, Y. Jang, J. Cho, M. Hwang and K. Cho, *Advanced Materials,* 2006, **18**, 719-723.
39 S. Wang, L. Dössel, A. Mavrinskiy, P. Gao, X. Feng, W. Pisula and K. Müllen, *Small,* 2011, **7**, 2841-2846.
40 E. Rabani, D. R. Reichman, P. L. Geissler and L. E. Brus, *Nature,* 2003, **426**, 271-274.
41 S. Rait, S. Kashyap, P. Bhatnagar, P. Mathur, S. Sengupta and J. Kumar, *Solar energy materials and solar cells,* 2007, **91**, 757-763.
42 D. Chirvase, J. Parisi, J. C. Hummelen and V. Dyakonov, *Nanotechnology,* 2004, **15**, 1317.
43 M. Reyes-Reyes, K. Kim and D. L. Carroll, *Applied Physics Letters,* 2005, **87**, 083506.
44 M. Campoy-Quiles, T. Ferenczi, T. Agostinelli, P. G. Etchegoin, Y. Kim, T. D. Anthopoulos, P. N. Stavrinou, D. D. Bradley and J. Nelson, *Nature materials,* 2008, **7**, 158-164.
45 T. Erb, U. Zhokhavets, G. Gobsch, S. Raleva, B. Stühn, P. Schilinsky, C. Waldauf and C. J. Brabec, *Advanced Functional Materials,* 2005, **15**, 1193-1196.
46 G. Li, V. Shrotriya, Y. Yao and Y. Yang, *Journal of Applied Physics,* 2005, **98**, 043704.

Table of Contents